

Testing and Modeling the Behavior of Concrete under Cyclic Tensile Loading

C. Kessler-Kramer

Deutsche Bahn AG (German Railway Construction Inc.), Karlsruhe, Germany

V. Mechtcherine

Technical University of Kaiserslautern, Kaiserslautern, Germany

H.S. Müller

University of Karlsruhe (TH), Karlsruhe, Germany

ABSTRACT: Based on the results of fracture mechanical and phenomenological investigations a new material law for concrete under cyclic tensile loading was developed. Its constitutive relations are based on a physically sound rheological-statistical model consisting of simple rheological elements. The verification of the model by means of a comparison between the results of numerical calculations and the corresponding experimental results showed a good agreement for various combinations of the decisive parameters.

Keywords: fatigue behavior, uniaxial tension, constitutive law, concrete, rheological model

1 INTRODUCTION

In practice the majority of concrete structures is exposed to more or less severe cyclic loadings, such as traffic loads, temperature changes, wind gusts and in some cases waves or vibrations due to operation of machinery.

Therefore, a profound knowledge of the fatigue behavior of concrete and concrete structures is indispensable for safety and economical reasons. Furthermore, appropriate constitutive laws are required in order to be able to analyze the formation and propagation of cracks in concrete as well as the deformation behavior or possibly a failure of concrete structures subjected to cyclic loading. Both topics mentioned above are addressed in this contribution.

2 EXPERIMENTAL PROGRAM

2.1 Fracture mechanical tests

In the experimental part of this study a series of deformation controlled uniaxial tensile tests on notched and unnotched concrete prisms was carried out for different combinations of the parameters under investigation.

Figure 1 shows a schematic view of the geometry of the two main types of specimens used for the uniaxial tensile tests and the geometry for the addi-

tionally performed three-point bend tests with a compensation of the beam deadweight.

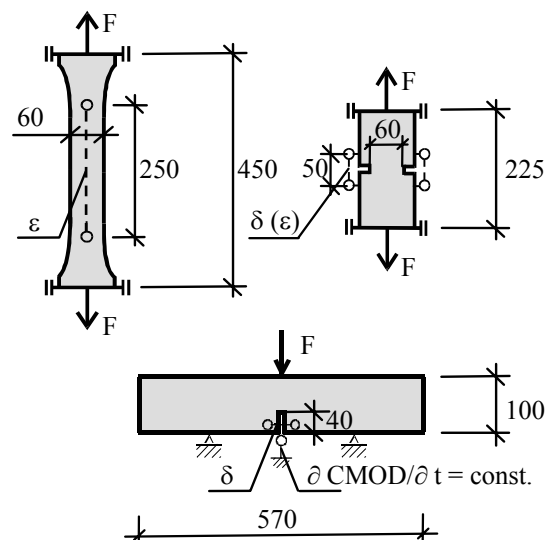


Figure 1. Geometrical dimensions of the investigated specimens (thickness of all three specimens $d = 100$; data in [mm]).

From the uniaxial tensile tests the functional dependences of the tensile strength f_t , the fracture energy G_F and the characteristic deformations of concrete from the strain rate (10^{-4} 1/s and 10^{-5} 1/s), the concrete grade (normal strength and high strength concrete, denoted as NSC and HSC), the

curing conditions (sealed and unsealed specimens) as well as the number of load cycles varying from 1 (monotonic loading) to 100,000 and 1 million (high-cycle fatigue) could be derived. On this basis and under consideration of the specific shape of obtained stress-deformation relations a new material law for concrete subjected to cyclic tensile loading was developed.

The three-point bend tests with deadweight compensation were necessary to provide data for the adjacent verification of the new material law. These tests were simulated applying the developed constitutive relations, and subsequently the experimental and numerical results were compared.

The test control in the fatigue experiments was realized by deformation control in contrast to the classical Wöhler fatigue experiments with a predefined lower and upper load limit. The increase of the total deformation within the measuring length corresponding to the crack opening is given by the deformation increment $\Delta\delta$, which was kept constant from cycle to cycle (i.e. $\Delta\delta = d\delta/dn = \text{const}$, where n = number of load cycles). When the preset value $\Delta\delta$ in the following cycle is reached the specimen is unloaded until the lower reversal point δ_{min} is attained. The lower reversal point δ_{min} was defined as a function of the lower load level $F_{min} = \text{const} = 0$ N.

Further details concerning the experimental program, especially the preparation of the specimen and the loading regime may be found in Kessler-Kramer et al. (2001) or Kessler-Kramer (2002).

As the main results in the uniaxial tension tests on the dog-bone shaped prisms it was found that the stress-strain relations for the HSC always run above the corresponding curves for the NSC, mainly due to the denser and more homogeneous microstructure of HSC. Furthermore, the shape of the σ - ε relations for the HSC in the ascending branch remains linear up to a higher stress level in comparison to the corresponding relations for the NSC.

With an increase of the strain rate by a factor of 10 higher values of the uniaxial tensile strength f_t , the Young's modulus E_0 and the elongation at failure ε_{tu} were measured. The observed strain rate dependency may be explained by considering the crack development in concrete as a function of time and agrees well with the data given by Mechtcherine et al. (1995) or the ACI Committee 446 (1995).

The experimental results obtained from the tests on the notched concrete prisms show particularly that with an increasing number of load cycles the net tensile strength f_m decreases (Fig. 2). However, in the low-cycle region up to 100 load cycles the f_m -values remain approximately constant. Note, that the values for f_m are taken from the related envelope curves in the case of cyclic tests (see also Fig. 4).

The strength values obtained for the unsealed specimens are lower than the corresponding values for the sealed specimens. This agrees well with the results obtained from the tests on the dog-bone shaped prisms and can be mainly explained by the fact that the hydration of the sealed specimens could reach a higher degree in the whole concrete prism whereas the unsealed specimens were allowed to desiccate at the surfaces. Further, the desiccation leads to pronounced moisture gradients throughout the cross section which finally results in eigenstresses and the formation of microcracks.

The effect of the strain rate in the experiments on the notched concrete prisms was found to be similar to that observed in the tests on the dog-bone shaped prisms.

In comparison to the values obtained for the normal strength concrete the net tensile strength of HSC is always higher, resulting in a higher storage of the energy due to elastic deformations.

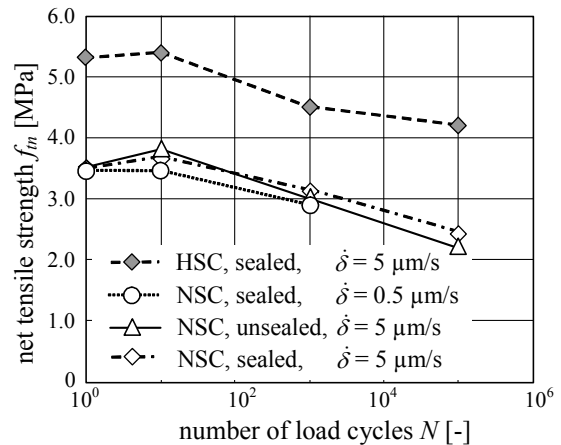


Figure 2. Effect of the number of load cycles to failure on the net tensile strength in tension tests on normal and high strength concrete for different deformation rates and curing conditions.

Figure 3 shows a decrease of the fracture energy G_F in the high-cycle fatigue tests with an increasing number of load cycles. Here, the G_F -values were calculated as the area under the measured stress-deformation curves. In the case of cyclic tests the envelope curves of the corresponding stress-deformation relations have been chosen. Therefore, a possible contribution of the area within the hysteric loops was not considered. Since the reduction of the investigated parameters with an increasing number of load cycles is approximately the same for HSC and NSC, it can be concluded that the effect of the fatigue loading is similar for both concretes.

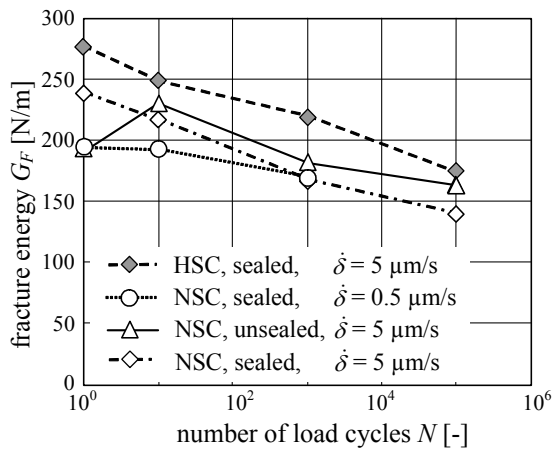


Figure 3. Effect of the number of load cycles to failure on the fracture energy in tension tests on normal and high strength concrete for different deformation rates and curing conditions.

The main finding in the experiments is that for an increasing number of load cycles the envelope curves of the σ - δ relations differ significantly from the corresponding monotonic curve, see Figure 4.

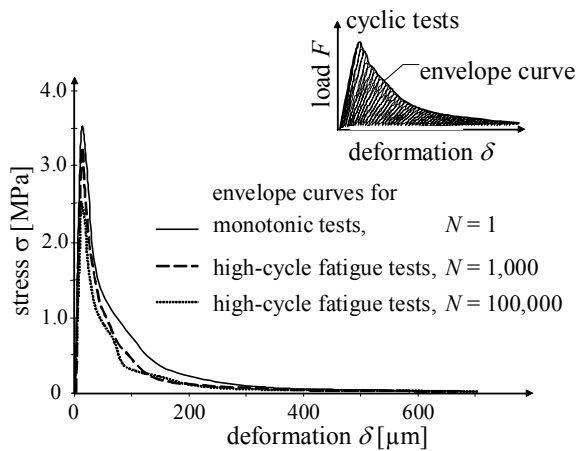


Figure 4. Envelope curves of the stress-deformation relations obtained from the monotonic and the high-cycle fatigue tests performed on sealed specimens made of NSC.

The ascending branches show approximately the same shape for all curves. Because of the lower f_m -values for the high-cycle fatigue tests (Fig. 2) these curves are below the curves for the monotonic and the low-cycle fatigue tests (the latter ones are not shown in Figure 4 for the reason of clearness) in the first, steeper part of the stress-deformation relation. This also leads to the lower G_F -values with an increasing number of load cycles (Fig. 3) which is mainly due to a lower energy consumption in this

part of the softening curve. Further, at these deformations the curves from the high-cycle fatigue tests are steeper than the curves from the monotonic and the low-cycle fatigue tests, see Figure 4. In the second, shallow part of the softening curve the average curves for the high-cycle fatigue becomes shallower and, when a deformation of about 150 μm is reached, nearly congruent to the curves for low cycle fatigue. The curve for the monotonic loading is slightly higher at this deformation region and coincides with the curves for the cyclic loading at a deformation of about 350 μm . Nevertheless, the contribution of the second part of the softening curve to the value of the fracture energy is limited, since it covers a minor amount of energy compared to the first part of the softening curve.

The mentioned observations clearly show that the conventional assumption of a unique envelope curve for the fatigue behavior of concrete cannot be maintained for high-cycle fatigue loading.

Further results for additionally investigated mechanical and fracture mechanical parameters such as miscellaneous deformations, characteristic length etc. under cyclic tensile loading may be found in Kessler-Kramer (2002).

2.2 Phenomenological investigations

2.2.1 Acoustic emission analysis

In order to gain more information on the process of the crack formation and propagation in concrete under cyclic loading phenomenological investigations were additionally performed by means of an acoustic emission (AE) analysis during fracture mechanical tests.

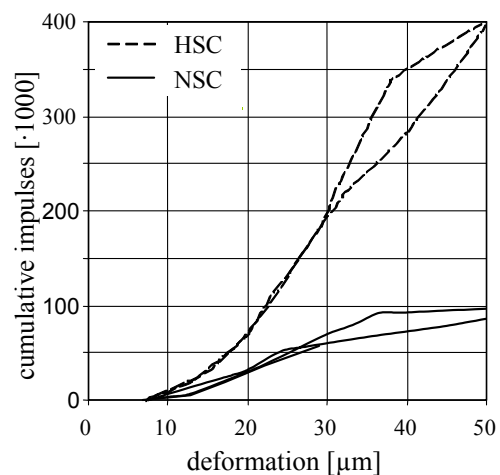


Figure 5. Effect of the concrete grade on the shape of the cumulative impulses via the deformation for low-cycle fatigue tests.

The concomitant analysis by means of acoustic emission resulting from the fracture process showed that the curves for the cumulative impulses, i.e. the amount of impulses within a specific time interval above a certain trigger threshold, obtained from the uniaxial tensile tests on HSC are well above the curves received from the tests on NSC (Fig. 5).

Figure 6 shows the effect of cyclic tensile loading on the shape of the curve of the cumulative impulses for the HSC for a number of loading cycles equal to 10. Additionally, the curves are shown for the case of cyclic tests considering just the acoustic emission during the deformation increments $\Delta\delta$, i.e. neglecting the signals during the deformations within the hysteretic loops (see dotted lines in Figure 6).

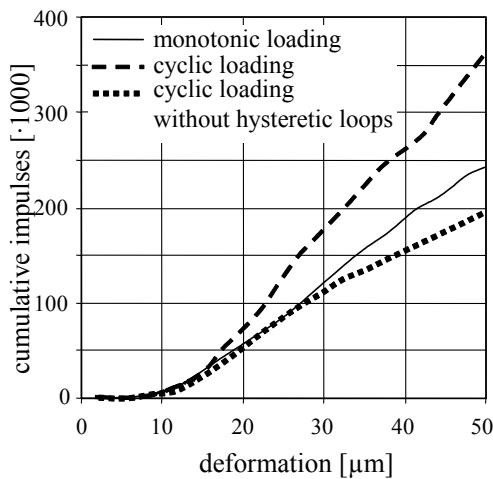


Figure 6. Average curves of the cumulative impulses via the deformation for HSC in monotonic and cyclic tension tests.

Up to a deformation of about 30 μm the curve for the monotonic loading matches the curve for the cyclic loading without hysteretic loops quite well. With further increasing crack propagation the cyclic tests provided lower acoustic emissions. However, in the case of cyclic tests with the consideration of the hysteretic loops higher values of the cumulative impulses could be obtained.

Thus it can be concluded that the damaging effects outside of the hysteretic loops are similar to those in the case of monotonic loading up to a crack opening of around 30 μm . The acoustic emission within the load cycles is mainly due to frictional effects as a result of the repeated opening and closing of the cracks with rough surfaces.

With further crack opening the damaging effects are shifted to the hysteretic loops, which can be recognized by the subsequently lower values of

the cumulative impulses in the cyclic tests without regarding the hysteretic loops (Fig. 6). Considering the nearly constant G_F -values for monotonic and low-cycle fatigue loading (Fig. 3) the damage due to a few load cycles can be neglected.

For high-cycle fatigue tests this detailed consideration of the individual deformation parts was not suitable due to the extremely low deformation increments per cycle. Nevertheless, it could be observed that the curves for the cumulative impulses in the case of high-cycle fatigue tests are far above the corresponding curves obtained from monotonic and low-cycle fatigue tests. In the case of high-cycle fatigue the damage within hysteretic loops takes place already before the peak load is reached. Therefore, in these tests lower f_m -values were obtained in comparison to monotonic or low-cycle fatigue tensile tests (Fig. 2). These additional damaging effects due to repeated loading might not be recognized until a certain number of load cycles has been performed.

Further results as well as a detailed description of the measurement technique, the used test set-up as well as the applied analytical evaluation may be found in Kessler-Kramer (2002).

2.2.2 Fractological investigations

After performing the tensile tests, the fracture surfaces of the tested concrete specimens were studied using projected fringes technique.

This technique is based on the phenomenon that height differences of the cracked concrete surfaces induce a lateral displacement of the projected strip pattern. Together with the geometrical data of the test set-up the phase shift of the projected fringes allows to obtain the contour information at intervals of 0.16 mm (giving a mesh of 375×625 data points for each failure surface). To avoid larger areas of receiving no information due to “shadow effects” a projection from two sides was necessary.

From the optical measurement data the roughness R_S and the fractal dimension D_{GS} were determined (Table 1). The roughness R_S was defined as the surface area measured with the finest resolution (0.16 mm) divided by the projected area. The determination of the fractal dimension D_{GS} was performed by means of the grid scaling method (Mechtcherine 2000).

As it can be seen from the results given in Table 1 an increase of the number of load cycles leads to an increase of both investigated parameters R_S and D_{GS} , i.e. the fracture surfaces become rougher indicating also a higher degree of the damage of concrete.

Table 1. Roughness and fractal dimension of concrete fracture surfaces of the concretes under investigation (standard deviations are given in parentheses).

Concrete grade; curing conditions; deformation rate; number of load cycles	Roughness R_S [-]	Fractal Dimension D_{GS} [-]
NSC; sealed; $\dot{\delta} = 5 \mu\text{m/s}$; $N = 1$	1.281 (0.003)	2.043 (0.005)
NSC; sealed; $\dot{\delta} = 5 \mu\text{m/s}$; $N = 10$	1.297 (0.017)	2.043 (0.004)
NSC; sealed; $\dot{\delta} = 5 \mu\text{m/s}$; $N = 1000$	1.325 (0.032)	2.050 (0.002)
NSC; sealed; $\dot{\delta} = 5 \mu\text{m/s}$; $N = 100,000$	1.335 (0.033)	2.051 (0.003)
NSC; unsealed; $\dot{\delta} = 5 \mu\text{m/s}$; $N = 1$	1.291 (0.017)	2.047 (0.001)
NSC; sealed; $\dot{\delta} = 0,5 \mu\text{m/s}$; $N = 1$	1.290 (0.030)	2.046 (0.004)
HSC; sealed; $\dot{\delta} = 5 \mu\text{m/s}$; $N = 1$	1.245 (0.027)	2.041 (0.003)

This result corresponds very well with the findings of the AE analyses, which showed higher values of the cumulative impulses for the fatigue tests in comparison with the monotonic tests, if the acoustic events “within” the hysteretic loops were considered (see Section 2.2.1).

Further, the use of an unsealed specimen as well as a lower deformation rate leads to higher values of the roughness R_S and the fractal dimension D_{GS} , whereas for the high strength concrete lower values of R_S and D_{GS} were found in comparison to the normal strength concrete.

3 MODELING THE CONCRETE BEHAVIOR

3.1 Rheological-Statistical Model

The experimental results obtained in this study restrict the validity of the existing constitutive relations to the range of low-cycle fatigue since they are completely based on the assumption that the monotonic stress-crack opening curve fits the envelopes for fatigue loading without considering the number of load cycles to failure, see e.g. Duda & König (1991) or Hordijk (1991).

Based on these results, a new constitutive law on the basis of a rheological-statistical model considering in particular the number of load cycles, time effects and the heterogeneity of concrete was currently developed (Fig. 7).

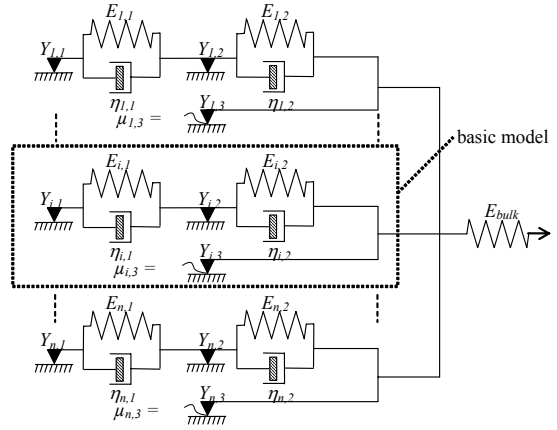


Figure 7. Rheological-statistical model for the description of the fatigue behavior of concrete under tensile loading.

The model consists of simple rheological elements like springs, friction blocks and dashpots representing the elastic, frictional and viscous deformation components of concrete. The selected basic model consists of two Kelvin-Voigt elements and three dashpots (framed with dotted lines in Fig. 7).

The hysteretic loops are described by a serial arrangement of two friction blocks and two Kelvin-Voigt elements. The dashpots $\eta_{i,1}$ and $\eta_{i,2}$ arranged parallel to the spring elements $E_{i,1}$ and $E_{i,2}$ enable to consider the rate dependency of concrete and to consider the effects due to the load history. The parallel arrangement of a further friction block $Y_{i,3}$ allows the modeling of the effect that loosened or pulled out aggregates or hardened cement paste particles may dislocate while the crack is open and lead to local tensile as well as compressive stresses in the case of unloading. Since this phenomenon just appears within the hysteretic loops and the induced stresses depend on the load history the associated friction coefficient $\mu_{i,3}$ is given as a function of the number of load cycles N (Fig. 7).

The complete model consists of n basic models arranged parallel with the parameters Y , E and η being statistically distributed and following an exponential function after Weibull. This approach considers the heterogeneity of concrete. The bulk behavior of the undamaged concrete is taken into account by an additional spring element E_{bulk} .

3.2 Constitutive Relations

The complete rheological-statistical model can transfer the stress σ given with Equation 1 as a function of the actual crack opening w under the condition of both serial arranged friction blocks $Y_{i,1}$

and $Y_{i,2}$ being in motion and transferring the full friction load. Thus Equation 1 is valid for monotonic loading as well as for the deformation increments $\Delta\delta$ outside the hysteretic loops in the case of cyclic loading (in other words the envelope curve, acc. to Fig. 4):

$$\sigma(w) = c_1 \cdot (\sigma_{Y1,0} + \sigma_{Y2,0}) \cdot f_{H1}(w) + c_2 \cdot (\sigma_{Y1,0} + \sigma_{Y2,0}) \cdot f_{H2}(w) \quad (1)$$

In Equation 1 $\sigma_{Y1,0}$ and $\sigma_{Y2,0}$ denote the transferable stresses of the first and the second friction elements, respectively and c_1 and c_2 are correlations coefficients. The functions $f_{H1}(w)$ and $f_{H2}(w)$ are the statistical distributions according to the theory of Weibull with different coefficients α , β and γ .

The transferable stress within the hysteretic loops can be calculated by adding the load carrying capacities of the second spring elements $E_{i,2}$, the second dash pots $\eta_{i,2}$ and the parallel arranged third friction elements $Y_{i,3}$ according to Equation 2:

$$\sigma(w) = c_1 \cdot [(w - w_2) \cdot k_2 + \frac{\eta_2}{l_{meas}} \cdot (\dot{w} - \dot{w}_2)] \cdot f_{H1}(w) + c_2 \cdot [(w - w_2) \cdot k_2 + \frac{\eta_2}{l_{meas}} \cdot (\dot{w} - \dot{w}_2)] \cdot f_{H2}(w) + \sigma_{Y3,0} \cdot f_{Y3}(w) \quad (2)$$

The displacement $w_2 = f(\eta_1, \eta_2, k_2)$ as well as the corresponding velocity \dot{w}_2 of the second friction elements $Y_{i,2}$ in Equation 2 are dependent whether the material is actually unloaded or reloaded. The parameter k_2 denotes the stiffness of the second spring elements, η_2 the viscosity of the second dash pots and l_{meas} the measuring length used in the experiments. $\sigma_{Y3,0}$ denotes the stresses transferable by the third friction elements and $f_{Y3}(w)$ the corresponding statistical distribution of a hyperbolic type.

To proceed from the developed material model to a constitutive material law the unknown model parameters in Equations 1 and 2 have to be determined by means of an appropriate inverse analysis. Thereby it could be concluded that the parameters β_2 , c_1 and c_2 are most suitable to reflect the relevant effects of the concrete grade, the strain rate, the curing conditions and the number of load cycles on the stress-crack opening relation in Equation 1. Equation 3 summarizes the coefficients from Equation 1 defined as constants and Equation 4 gives the corresponding values of the parameters for describing the hysteretic loops using Equation 2.

$$\alpha_1 = \alpha_2 = 0 \quad ; \quad \beta_1 = 0.02 \quad ; \quad \gamma_1 = 2.0 \quad \text{and} \quad \gamma_2 = 1.2 \quad (3)$$

$$\sigma_{Y1,0} = 2/3 \cdot f_t \quad ; \quad \sigma_{Y2,0} = 1/3 \cdot f_t \quad ; \quad \sigma_{Y3,0} = 0.05 \cdot f_t \quad ; \quad k_2 = (167 - 5 \cdot \log N) \cdot f_t \quad (4)$$

Further details concerning the determination of the model parameters and an additional simplification of the constitutive law by replacing the description of the hysteretic loops with a single relation for the actual compliance as a function of the crack opening may be found in Kessler-Kramer (2002).

As a last step for the modeling the functional dependences of the f_t , E_0 , ε_{tu} and G_F -values from the investigated parameters found in the experimental part of this study had to be formulated. For this purpose the functional expressions were chosen similar to those proposed by the CEB-FIP Model Code 1990 (1993).

In the following only the effect of the concrete grade will be described exemplary. Hereby the effect of the concrete grade on the uniaxial tensile strength f_t as well as on the Young's Modulus E_0 could be experimentally determined well according to the formulas given in MC 90 (1993). Therefore, these functional dependencies could be adopted directly as given with the Equations 5 and 6:

$$f_t = 1.40 \cdot (f_c / 10)^{2/3} \quad (5)$$

$$E_0 = 2.15 \cdot 10^4 \cdot (f_c / 10)^{1/3} \quad (6)$$

where f_c = characteristic compressive strength (all parameters in [MPa]).

In contrast to this the formulation for the fracture energy G_F is deviating from the formula given in MC 90 (1993).

$$G_F = 157 \cdot (f_c / 10)^{0.215} \quad (7)$$

The derived Equation 7 is resulting in higher values for the fracture energy G_F than the formula given in MC 90 (1993) especially for normal strength concrete. This can be traced back mostly to an optimized test set-up and the use of non-rotatable boundary conditions in the own tensile tests.

According to Hooke's law the strain at the peak stress ε_{tu} is given with the Equations 5 and 6:

$$\varepsilon_{tu} = 65 \cdot 10^{-6} \cdot (f_c / 10)^{1/3} \quad (8)$$

In contrast to Equation 8 MC 90 (1993) provides a constant value for ε_{tu} of about $150 \cdot 10^{-6}$. This constant value for the strain at the peak stress in tensile tests could be already disproved in experiments by many researchers (see e.g. Mechtcherine, 2000).

3.3 Calibration and verification of the new constitutive laws

The numerical investigation described in this chapter is restricted to the calibration and the verification of the new developed constitutive law.

In a first step it was necessary to calibrate the free parameters of the model on the basis of the results obtained from the axial tests as described in Chapter 2. Here the envelope curves of the stress-crack opening relations as well as single hysteretic loops were calculated for different combinations of parameters influencing the softening behavior of concrete under monotonic and cyclic loading.

Figure 8 shows the stress-crack opening relations obtained from the tensile tests on notched prisms in comparison with the curve according to Equation 1. The curves were determined for sealed concrete prisms made of NSC and tested under monotonic loading with a deformation rate of $5 \mu\text{m/s}$. The free parameters of the model were determined as $\beta_2 = 0.1$, $c_1 = 0.0155$ and $c_2 = 3 \cdot c_1 = 0.0465$. The curves agree very well up to a crack opening of about $250 \mu\text{m}$. Afterwards the transferable stress is slightly underestimated by the curve according to Equation 1 leading to a more conservative estimation. In view of the scatter of the single results this can be taken as well justified. A more exact reproduction of the experimentally determined stress-crack opening curve could be realized by the aid of a further Weibull function or the choice of a different function to reflect the scatter. Nevertheless this would lead to a more complex mathematical formulation and a reduced transparency of the failure mechanisms occurring in concrete cracking.

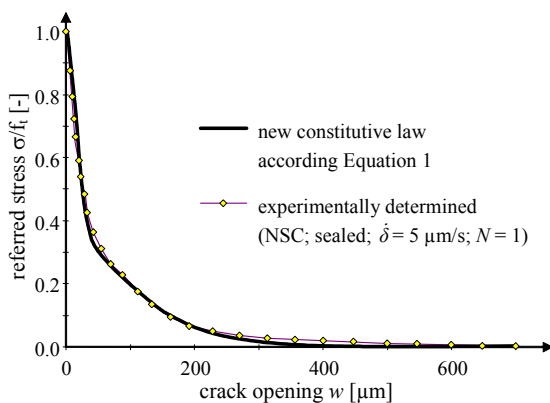


Figure 8. Comparison of the envelope curves of the stress-crack opening relations obtained from the experiments and the new constitutive law for monotonic tensile tests performed on sealed concrete prisms made of NSC.

In Kessler-Kramer (2002) further comparisons of the envelope curves for other parameters like the concrete grade, the curing conditions, the deformation rate and the number of load cycles to failure are given. All these curves given by the new rheological model coincide very well with the experimentally determined curves.

If individual hysteretic loops are considered instead of the envelopes of the stress-crack opening relations, the curves can be obtained as given in Figure 9 for three selected loops. Figure 9 clearly shows that the new developed constitutive law is able to describe the unloading as well as the reloading paths of a stress-crack opening relation for low-cycle fatigue loading. The same positive result has been received for high-cycle fatigue loading.

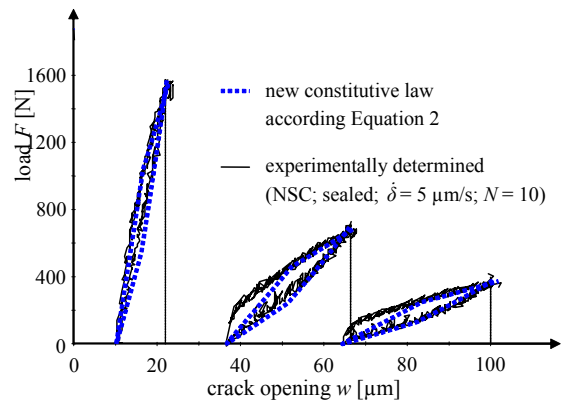


Figure 9. Comparison of the hysteretic loops obtained from the experiments with the corresponding curves given by the new constitutive law (here for low-cycle fatigue tests performed on sealed concrete prisms made of NSC).

Due to the bilinear description in the developed model the reloading path shows a little deviation immediately after the lower reversal point is passed. This minor discrepancy can be traced back to the fact, that the effects due to the dislocation of the loosened or pulled out aggregates or cement paste particles while the crack is open, was considered in the model by the parallel arranged friction elements in a rather rough manner (see section 3.1).

A further optimization of the model prediction could be reached using a modified arrangement of the rheological elements. However, this would lead again to a reduced transparency of the model, which is indeed one of the outstanding advantages of the modeling by using rheological elements.

To verify the new constitutive law a simple application was chosen: a prediction of the structural behavior of small-sized concrete members.

For this reason the three-point bend tests (see Fig. 1) were simulated numerically applying the new developed material law. Since the results of these tests had not been considered for the derivation of the constitutive relations as described above, they were suitable for the verification of the results of a numerical calculation by means of the finite element method.

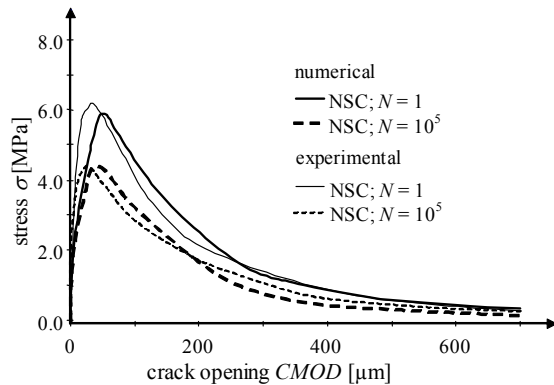


Figure 10. Envelope curves of the stress-CMOD (crack mouth opening displacement) relations obtained from the numerical calculations as well as from the monotonic and the high-cycle fatigue three-point bend tests.

As it can be easily seen from Figure 10, the FE simulation applying the new constitutive law provided a rather good prediction of the concrete behavior observed experimentally. Only the transferable stress in the first, steeper part of the descending branch in the stress-crack opening diagram is slightly overestimated. A good prediction for the load-CMOD relations could also be observed for the other parameters such as strain rate, concrete grade and curing conditions (Kessler-Kramer, 2002).

4 CONCLUSIONS

In this contribution the determination of characteristic parameters of concrete under monotonic and cyclic loading by means of an extensive experimental investigation as well as the derivation of the relevant parameters for adequate constitutive laws were addressed.

In the experimental part of the study it was found that with an increasing number of load cycles, the axial tensile strength, the deformation at the peak load, the critical crack opening, the fracture energy and the characteristic length for both normal strength and high strength concrete decrease significantly.

For the first time it could be shown that the envelope curves of the stress-deformation relations di-

verge more and more evidently from the corresponding monotonic curve as the number of load cycles increases. This restricts the validity of the existing constitutive relations to the range of low-cycle fatigue as they are completely based on the assumption of a unique envelope curve being identical to the stress-crack opening relation for monotonic loading.

During the fracture mechanical experiments a measurement of acoustic emissions were performed in order to quantify the process of the crack formation in concrete. Further, after the tests the fracture surfaces were studied using projected fringes technique, which enabled to obtain a more profound insight into the mechanisms of the propagation of cracks in concrete under cyclic loading.

Based on the results of fracture mechanical and phenomenological investigations a new material law for concrete under cyclic tensile loading was developed. Its constitutive relations are founded on a physically sound rheological-statistical model consisting of simple rheological elements. The functional dependences of the decisive model parameters from the affecting parameters were formulated similar to the equations proposed in CEB-FIP Model Code 1990 (1993). The verification of the model by comparing the results of numerical calculations of the bend tests with the corresponding experimental results showed a good agreement for various combinations of the decisive parameters.

5 REFERENCES

- ACI Committee 446. 1995. State-of-the-Art Report on *Dynamic Fracture*, Report ACI 03.95 – R8860.
- Duda, H. & König, G. 1991. Rheological Material Model for the Stress-Crack Width Relation of Concrete under Monotonic and Cyclic Tension. *ACI Materials Journal*, Vol. 88, No. 3.
- Hordijk, D. A. 1991. *Local Approach to Fatigue of Concrete*. Dissertation. Delft University of Technology, Delft.
- Kessler-Kramer, C. 2002. *Tensile Structural Behavior of Concrete under Fatigue Loading*. Institute of Concrete Structures and Building Materials, University of Karlsruhe, Vol. 49 (in German).
- Kessler-Kramer, C., Mechtcherine, V. & Müller, H.S. 2001. Fatigue Behavior of Concrete in Tension. *Proc. 4th Intern. Conf. on Fracture Mechanics of Concrete and Concrete Structures*, Cachan, France, May 2001.
- Mechtcherine, V. 2000. *Fracture Mechanical and Fractological Investigations on the Formation and Propagation of Cracks in Concrete*. Institute of Concrete Structures and Building Materials, University of Karlsruhe, Vol. 40 (in German).
- Mechtcherine, V., Garrecht, H. & Hilsdorf, H.K. 1995. Effect of Temperature and Loading Rate on Fracture Behaviour of Concrete Subjected to Uniaxial Tension. *Proc. 2nd Intern. Conf. on Fracture Mechanics of Concrete and Concrete Structures*, F.H. Wittmann (ed.), Aedificatio Publishers.
- CEB – Comité Euro-International du Béton. 1993. CEB - FIP Model Code 1990, *CEB Bulletin D'Information*, No. 213/214, Lausanne.